Azimuthal field instability in a confined ferrofluid

Eduardo O. Dias* and José A. Miranda†
Departamento de Física, Universidade Federal de Pernambuco, Recife, Pernambuco 50670-901 Brazil
(Received 30 December 2014; published 27 February 2015)

We report the development of interfacial ferrohydrodynamic instabilities when an initially circular bubble of a nonmagnetic inviscid fluid is surrounded by a viscous ferrofluid in the confined geometry of a Hele-Shaw cell. The fluid-fluid interface becomes unstable due to the action of magnetic forces induced by an azimuthal field produced by a straight current-carrying wire that is normal to the cell plates. In this framework, a pattern formation process takes place through the interplay between magnetic and surface tension forces. By employing a perturbative mode-coupling approach we investigate analytically both linear and intermediate nonlinear regimes of the interface evolution. As a result, useful analytical information can be extracted regarding the destabilizing role of the azimuthal field at the linear level, as well as its influence on the interfacial pattern morphology at the onset of nonlinear effects. Finally, a vortex sheet formalism is used to access fully nonlinear stationary solutions for the two-fluid interface shapes.

DOI: 10.1103/PhysRevE.91.023020 PACS number(s): 47.65.Cb, 47.15.gp, 47.54.−r, 47.20.Ma

I. INTRODUCTION

Ferrofluids are colloidal suspensions of nanometer-sized magnetic particles suspended in a nonmagnetic carrier fluid [1,2]. This particular type of magnetic fluid behaves superparamagnetically and can easily be manipulated with external magnetic fields. The combined action of hydrodynamic and magnetic forces makes ferrofluids a remarkable material to study a variety of interfacial instabilities and pattern formation processes [3]. One iconic example of pattern-forming phenomena in ferrofluids is the Rosensweig instability [4]. It occurs when an initially flat free surface of a ferrofluid film is subjected to a uniform, perpendicular magnetic field generated by a pair of Helmholtz coils. The competition between magnetic, gravitational, and capillary forces results in the rising of a visually striking, three-dimensional (3D) array of spiky structures (the Rosensweig's peaks) growing from the liquid-free surface. Since then, various aspects related to the form of the peaks and their nontrivial dynamic behavior have been scrutinized by theory, simulations, and experiments (see, for instance, Refs. [5–9], and references therein).

Another popular event in ferrohydrodynamics, known as the conical meniscus instability, refers to the formation of a static meniscus profile when an originally horizontal 3D layer of ferrofluid encloses a vertical current-carrying wire [10]. This particular setup is quite simple and generates an azimuthal magnetic field that turns around the wire. As opposed to the perpendicular field case studied in the development of the Rosensweig's peaks, the azimuthal field configuration produces a magnetic force directed radially inward. This force tends to attract the evolving ferrofluid toward the current-carrying wire, making the magnetic fluid to lift it, and resulting in the establishment of a curved ferrofluid meniscus. Since the seminal work of Ref. [10] investigators have carried out theoretical and experimental studies in order to determine the precise shape of the curved meniscus in both the absence and presence of surface tension effects [11–14]. Interestingly, the azimuthal magnetic field configuration produced by a straight current-carrying wire has also been used to examine the dynamics of solitons propagating on cylindrical ferrofluid surfaces surrounding the wire. There is a recent example in the literature in which theoretical predictions [15–17] about solitary wave propagation in ferrofluids has been realized experimentally [18].

Researchers have also analyzed how the perpendicular and azimuthal magnetic fields discussed above act on ferrofluids confined in the effectively 2D geometry of a Hele-Shaw cell. The Hele-Shaw apparatus [19,20] consists of two parallel glass plates separated by a narrow gap, where the ferrofluid can flow under the action of an applied magnetic field [2,3]. In contrast to the legitimately 3D free surface situation, the action of a magnetic field perpendicular to the plates of a Hele-Shaw cell containing an initially circular ferrofluid droplet encircled by a nonmagnetic fluid does not lead to peak formation. Instead, the applied field tends to align the tiny magnetic moments in the ferrofluid in a direction perpendicular to the plates. Consequently, these magnetic moments repel each other within the plane of the Hele-Shaw cell, and the two-fluid interface starts to distort. On the other hand, the surface tension between the fluids tends to stabilize the interface. The interplay between these two forces ultimately leads to the emergence of mazelike, multiply bifurcated structures, where a labyrinth-type pattern is formed. This characterizes the celebrated labyrinthine ferrofluid instability [21–24].

A considerably different scenario arises when a circular ferrofluid droplet, surrounded by a nonmagnetic fluid, is placed in a Hele-Shaw cell and subjected to an azimuthal magnetic field produced by current-carrying wire. In this context, the wire is normal to the cell plates and passes through the center of the ferrofluid droplet. As noted earlier, the azimuthal magnetic field generates a radial magnetic body force pointing inward, attracting the ferrofluid droplet toward the wire. Under such circumstances both surface tension and magnetic forces tend to stabilize the fluid-fluid interface. This azimuthal field stabilizing strategy has been proven effective to control interfacial instabilities in ferrofluids under centrifugally induced fingering in rotating Hele-Shaw cells [25–27], as well as during the stretch

*eduardodias@df.ufpe.br
†jme@df.ufpe.br

flow of thin ferrofluid films in the lifting Hele-Shaw flow setup [28,29].

In this work we study a still unexplored aspect of the azimuthal magnetic field configuration in Hele-Shaw geometry. More specifically, we consider the influence of the azimuthal field on the fluid-fluid interface, now assuming that a viscous ferrofluid is the outer fluid, while the inner fluid is inviscid and nonmagnetic. The interesting facet of the problem resides on the fact that in this situation the azimuthal field acts to *destabilize* the interface separating the fluids, offering the possibility of investigating innovative dynamical and pattern-forming behaviors.

It should be noted that, due its simplicity, the azimuthal magnetic field offers plenty of room to analytical treatment of the rising interfacial phenomena. This is in contrast to what happens in the perpendicular magnetic field case, where destabilization relies on complicated demagnetizing effects that usually defy the analytical treatment of the system, mainly during nonlinear stages of the dynamics. Here we tackle the ferrohydrodynamic problem analytically: first, a perturbative mode-coupling approach [30] is employed to access relevant features of the time-evolving interface up to quadratic nonlinearities. This allows one to examine the linear stability of the problem, as well as the most salient morphological characteristics of the two-fluid interface at the onset of nonlinear effects. Fully nonlinear features of the interface are also studied, via a vortex sheet approach [31], leading to the determination of stationary solutions for the interface shape.

II. LINEAR AND WEAKLY NONLINEAR REGIMES

A. Governing equations

Figure 1 illustrates an initially circular bubble (radius R) of an inviscid, nonmagnetic fluid surrounded by a ferrofluid

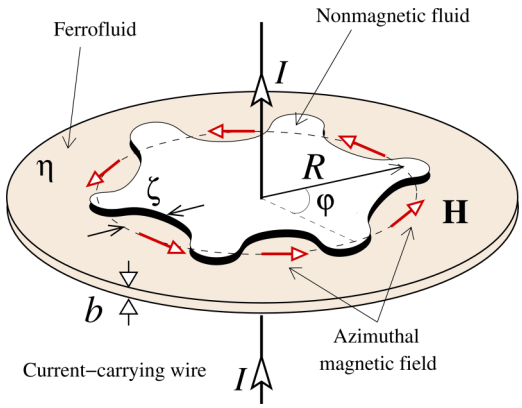

FIG. 1. (Color online) Representative sketch of the physical system: Hele-Shaw cell of thickness b containing an initially circular bubble (radius R) of an inviscid, nonmagnetic fluid surrounded by a ferrofluid of viscosity η. The in-plane azimuthal magnetic field $\mathbf{H}$ is produced by a long wire carrying an electric current I. The wire is perpendicular to the cell plates and passes through the center of the initially circular fluid-fluid interface. The azimuthal field destabilizes the two-fluid interface, deforming the circle with perturbation amplitude $\zeta = \zeta(\varphi,t)$, where φ denotes the azimuthal angle.

of viscosity η. Both fluids are incompressible and are located between two narrowly spaced flat plates of a Hele-Shaw cell of thickness b. The surface tension at the fluid-fluid interface is denoted by σ. We consider the action of an azimuthal magnetic field produced by a long, straight, current-carrying wire that is perpendicular to (coaxial with) the plates of the Hele-Shaw cell,

$$\mathbf{H} = \frac{I}{2\pi r}\hat{\mathbf{e}}_{\varphi}. \tag{1}$$

The electric current is represented by I, r is the radial distance from the origin of the coordinate system (located at the center of the cell), and $\hat{\mathbf{e}}_{\varphi}$ is a unit vector in the azimuthal direction. The azimuthal angle in the plane of the cell is denoted by φ. A magnetic body force $\sim\nabla H$, where $H = |\mathbf{H}|$, acts on the ferrofluid pointing in the inward radial direction [1,25].

While surface tension tends to keep the two-fluid interface circular, the magnetic force induced by the azimuthal magnetic field (1) acts to deform it. In the framework of our second-order perturbative approach, we describe the deformed interface shape as $\mathcal{R}(\varphi,t) = R + \zeta(\varphi,t)$, where $\zeta(\varphi,t) = \sum_{n=-\infty}^{+\infty} \zeta_n(t)\exp(in\varphi)$ represents the net interface perturbation with Fourier amplitudes $\zeta_n(t)$ and integer azimuthal wave numbers n. The zeroth mode is included in the Fourier expansion to keep the area of the perturbed shape independent of the perturbation ζ [30].

For the effectively two-dimensional geometry of the Hele-Shaw cell, the dynamics of the interface is governed by a modified Darcy's law for the gap-averaged velocity [21,24,25]

$$\mathbf{v} = -\frac{b^2}{12\eta}\nabla\Pi. \tag{2}$$

The generalized pressure $\Pi = p - \Psi$ contains both the pressure p and a magnetic pressure represented by a scalar potential $\Psi = \mu_0\chi H^2/2$, where the linear relationship $M = \chi H$ has been used, with χ denoting a constant magnetic susceptibility. Note that for the nonmagnetic fluid $\chi = 0$ and $\Psi = 0$.

From Eq. (2) and the incompressibility condition $\nabla\cdot\mathbf{v} = 0$ it can be verified that the velocity potential ϕ ($\mathbf{v} = -\nabla\phi$) obeys Laplace's equation. The problem is then specified by the augmented pressure jump boundary condition [1,2]

$$p|_{r=\mathcal{R}} = -\left[\sigma\kappa + \tfrac{1}{2}\mu_0(\mathbf{M}\cdot\hat{\mathbf{n}})^2\right]_{r=\mathcal{R}}, \tag{3}$$

with $\hat{\mathbf{n}} = \nabla[r - \mathcal{R}(\varphi,t)]/|\nabla[r - \mathcal{R}(\varphi,t)]|$ denoting the unit normal vector at the interface, plus the kinematic boundary condition [20]

$$\frac{\partial\mathcal{R}}{\partial t} = \left[\frac{1}{r^2}\frac{\partial\mathcal{R}}{\partial\varphi}\frac{\partial\phi}{\partial\varphi} - \frac{\partial\phi}{\partial r}\right]_{r=\mathcal{R}}, \tag{4}$$

which connects the velocity of the ferrofluid with the motion of the interface itself. The first term on the right-hand side of Eq. (3) represents the usual contribution related to surface tension and interfacial curvature κ. The second term is the so-called magnetic normal traction [1,2,27,28], which considers the influence of the normal component of the magnetization at the interface. This additional term will have an important role in determining the shape of the rising interfacial patterns under an azimuthal magnetic field.

Following canonical steps performed in previous weakly nonlinear studies for Hele-Shaw flows [28,30], first we define

Fourier expansions for the velocity potential. Then we express the Fourier coefficients of the velocity potential in terms of the perturbation amplitudes ζ_n by considering condition (4). Substituting these relations, and the pressure jump condition Eq. (3) into Darcy's law Eq. (2), always keeping terms up to second order in ζ, and Fourier transforming, we find the *dimensionless* equation of motion for the perturbation amplitudes (for $n \neq 0$)

$$\dot{\zeta}_n = \lambda(n)\zeta_n + \sum_{n' \neq 0} [F(n,n')\zeta_{n'}\zeta_{n-n'} + G(n,n')\dot{\zeta}_{n'}\zeta_{n-n'}], \quad (5)$$

where the overdot represents a total time derivative with respect to time,

$$\lambda(n) = |n|[\chi N_B - (n^2 - 1)] \quad (6)$$

denotes the time-independent linear growth rate, and

$$N_B = \frac{\mu_0 I^2}{4\pi^2 \sigma R} \quad (7)$$

is a magnetic Bond number that measures the ratio of magnetic and surface tension forces. The functions $F(n,n')$ and $G(n,n')$ are the second-order mode-coupling terms given by

$$F(n,n') = -|n|\left\{\frac{3}{2}\chi N_B\left[1 + \frac{1}{3}\chi n'(n' - n)\right] + \left[1 - \frac{n'}{2}(3n' + n)\right]\right\} \quad (8)$$

and

$$G(n,n') = |n|[1 - \mathrm{sgn}(nn')] - 1. \quad (9)$$

In Eq. (9) the sign function sgn equals ± 1 according to the sign of its argument. In Eq. (5) lengths and time are rescaled by R and $(12\eta R^3)/(b^2\sigma)$, respectively. From this point onward, we work with the dimensionless version of the equations. We stress that in the presentation of our theoretical results, we make sure that the values of all relevant dimensionless quantities we utilize are consistent with realistic physical parameters related to existing azimuthal magnetic field arrangements and material properties of ferrofluids [1,2,10–18].

B. Discussion of linear and weakly nonlinear results

In this section we utilize Eq. (5) to analyze the interfacial instability generated by the azimuthal magnetic field at early stages of the interface dynamics. The beginning of the fingering process occurs when a small initial disturbance at the ferrofluid interface is forced by the external magnetic field to grow toward the center of the nonmagnetic bubble. This initial behavior can be described by a linear stability analysis that considers just the contribution of the first term on the right-hand side of Eq. (5), leading to a simple differential equation $\dot{\zeta}_n = \lambda(n)\zeta_n$. One can readily see that a positive growth rate $\lambda(n)$ results in an unstable ferrofluid interface. Therefore, from Eq. (6) we conclude that the magnetic contribution, quantified by the magnetic Bond number N_B and by the magnetic susceptibility χ, induces a positive growth rate and, consequently, destabilizes the interface. Nonetheless, the second term in Eq. (6), which comes from the surface tension effect, tends to drive $\lambda(n)$ negatively, favoring the damping of any disturbances caused by the external field. It is worth noting that, since for ferrofluids the magnitude of the magnetic susceptibility can be as large as 60 or 70, it is perfectly possible to induce fingering with magnetic Bond numbers that are not necessarily large (e.g., $0 < N_B < 3$).

Another relevant piece of information can be extracted from the linear stability analysis. It refers to the linear prediction for the typical number of fingers formed at the interface during early stages of the pattern formation process. This quantity is given by the fastest growing mode, and it can be obtained by setting $[d\lambda(n)/dn]|_{n=n^{\lambda}_{\max}} = 0$. This leads to a pretty simple form for $n^{\lambda}_{\max}$ given by

$$n^{\lambda}_{\max} = \sqrt{\tfrac{1}{3}(1 + \chi N_B)}. \quad (10)$$

By inspecting Eq. (10), it is evident that the linear approach predicts that the typical number of fingers increases with the square root of N_B, where its growth is more accentuated for larger values of χ. Therefore, one might control the number of fingers at early linear stages of the dynamics by either manipulating the electric current on the wire (i.e., by tuning N_B) or by choosing an appropriate ferrofluid with a convenient susceptibility. However, it is important to stress that depending on the role played by the nonlinear effects, the growth rate, and, consequently, $n^{\lambda}_{\max}$, may not offer a good estimate for the number of emerging fingers. This important issue will be discussed below.

In order to extract more information about the emerging ferrofluid patterns, we turn our attention to the weakly nonlinear stage. Now we focus on assessing the most salient features of the patterns' *morphology* induced by the azimuthal magnetic field. It should be pointed out that such morphological characteristics cannot be predicted by a purely linear stability analysis of the system. The search for key nonlinear morphological aspects can be performed by making use of the full mode-coupling equation (5). In particular, we concentrate our attention on a fundamental mechanism of pattern formation in Hele-Shaw cells, related to the finger tip-splitting phenomenon [20]. Originally, finger tip-splitting events have been studied in the context of injection-driven radial Hele-Shaw flows [32–35] where the tip of the evolving fingers exhibited a tendency to get wider and wider and eventually went through a bifurcation process, where a single finger splits into two smaller ones. This finger duplication process may influence the proper counting of the fingers at the weakly nonlinear regime.

To give a flavor of how the mode-coupling approach can provide very useful information about finger tip-broadening and finger tip-splitting phenomena, we proceed by following the procedure originally implemented in Ref. [30] and consider the coupling of just a small number of Fourier modes. For convenience, we rewrite Eq. (5) in terms of cosine and sine modes, where the cosine $a_n = \zeta_n + \zeta_{-n}$ and sine $b_n = i(\zeta_n - \zeta_{-n})$ amplitudes are real valued. Without loss of generality we choose the phase of the fundamental mode so $a_n > 0$ and $b_n = 0$. In this approach, finger tip broadening, and finger tip splitting are described by considering the influence of a fundamental mode n on the growth of its first harmonic $2n$ [30].

Writing the equations of motion for the harmonic mode we have

$$\dot{a}_{2n} = \lambda(2n)a_{2n} + \tfrac{1}{2}T(2n,n)a_n^2, \tag{11}$$

$$\dot{b}_{2n} = \lambda(2n)b_{2n}, \tag{12}$$

where the finger tip function is defined as

$$\begin{aligned} T(2n,n) &= F(2n,n) + \lambda(n)G(2n,n) \\ &= |n|[\chi N_B(\chi n^2 - 4) + 6n^2 - 3]. \end{aligned} \tag{13}$$

Since the growth of the sine mode b_{2n} is uninfluenced by a_n and does not present second-order couplings, we focus on the growth of the cosine mode a_{2n} which is given by Eq. (11).

It is known that the function $T(2n,n)$ dictates the finger tip behavior [30,36]. From Eq. (11), notice that if $T(2n,n) > 0$, the term of order a_n^2 drives the growth of a_{2n} positively, leading to inward pointing finger tip broadening. For large magnitudes of the finger tip function, the nonlinear term can eventually promote the tip splitting of the inward pointing fingers of the ferrofluid. The same argument is valid if $T(2n,n) < 0$, where the tendency toward broadening of the outward pointing fingers is observed. From Eq. (13) it is easily seen that in our current problem $T(2n,n)$ is always positive for $n > 1$, regardless the value of N_B and for χ of order 1. In addition, notice that the magnitude of the finger tip function increases linearly with N_B, and its growth is more significant for higher values of the susceptibility. These findings indicate that by increasing N_B and χ, it is possible to observe a broadening or even a bifurcation process of the inward moving fingers of the ferrofluid at early nonlinear stages of the pattern formation process.

The illustrative analysis we performed above regarding the development of tip broadening and splitting of the invading ferrofluid fingers, used the coupling of just two particular Fourier modes. At this point, we wish to verify the validity and generality of these important results obtained from the finger tip function analysis. This is done by employing a more quantitative approach involving the nonlinear interaction among various Fourier modes. In other words, instead of examining the sole interaction between fundamental and first harmonic modes, we consider the participation and interplay of all linearly unstable Fourier modes [i.e., those for which $\lambda(n) > 0$]. In this general scenario, we have to solve the weakly nonlinear equation (5) consistently up to second-order accuracy. Substituting the linear solution

$$\zeta_n^{\text{lin}}(t) = \zeta_n(0)\exp\{\lambda(n)t\} \tag{14}$$

into the second-order terms on the right-hand side of Eq. (5), we obtain

$$\begin{aligned} \dot{\zeta}_n = \lambda(n)\zeta_n + \sum_{n'\neq 0}[F(n,n') + \lambda(n')G(n,n')]\zeta_{n'}(0)\zeta_{n-n'}(0) \\ \times \exp\{[\lambda(n-n') + \lambda(n')]t\}, \end{aligned} \tag{15}$$

where $\lambda(n-n')$ and $\lambda(n')$ correspond to the linear growth rate related to the modes $n-n'$ and n', respectively. Notice that Eq. (15) is a first-order linear differential equation for which a closed form solution can be written as

$$\begin{aligned} \zeta_n(t) = \zeta_n(0)\exp\{\lambda(n)t\} \\ + \sum_{n'\neq 0}\zeta_{n'}(0)\zeta_{n-n'}(0)\left[\frac{F(n,n') + \lambda(n')G(n,n')}{\lambda(n-n') + \lambda(n') - \lambda(n)}\right] \\ \times \Big[\exp\{[\lambda(n-n') + \lambda(n')]t\} - \exp\{\lambda(n)t\}\Big]. \end{aligned} \tag{16}$$

The analytical weakly nonlinear solution (16) allows the explicit consideration of the coupling of an arbitrary number of Fourier modes. From Eq. (16), one can easily obtain the equivalent weakly nonlinear solutions for the cosine and sine modes and then examine the evolution of the mode amplitudes as well as the shape of the resulting interface. Figure 2 plots the normalized Fourier amplitudes ($|\zeta_n|/|\zeta_{n_{\max}}|$) as a function of the modes n for three values of N_B: 0.15, 0.7, and 2.8. Here $|\zeta_n| = \sqrt{|a_n|^2 + |b_n|^2}/2$, $|\zeta_{n_{\max}}|$ denotes maximum amplitude ($n_{\max}$ is the mode of maximum amplitude), and $\chi = 70$. The plots are produced at the following final times: (a) 0.69, (b) 0.57, (c) 0.07, (d) 0.053, (e) 0.0083, and (f) 0.0055. These final times are determined so the condition of validity of our perturbative approach $|\zeta|/R \ll 1$ is obeyed.

In the insets we present the corresponding final interface shapes, where random phases have been attributed to each mode n, where $0 \leqslant n \leqslant 30$. Note that Figs. 2(a), 2(c), and 2(e) are obtained by using the linear stability theory, where just the linear term on right-hand side of Eq. (16) is taken into account. On the other hand, Figs. 2(b), 2(d), and 2(f) are plotted considering all terms in the weakly nonlinear solution (16).

By inspecting Figs. 2(a), 2(c), and 2(e) for the linear amplitudes we find that the number of resulting fingers, here given by the mode with maximum amplitude $n_{\max}$, increases with N_B consistently with the expression of the fastest growing mode $n_{\max}^{\lambda}$ (10). However, when nonlinear effects are taken into consideration [Figs. 2(b), 2(d), and 2(f)], we verify that the final number of fingers duplicates if compared to the number given by the purely linear prediction. Despite the fact that we have multiple interacting modes, in terms of the ultimate shape of the patterns, everything works as if we had a "fundamental mode" given by $n_{\max}$ and a nonlinearly selected, dominant "first harmonic" associated to $2n_{\max}$.

This interesting nonlinear result, valid for the interaction of multiple Fourier modes, is indeed in line with the finger tip function mechanism discussed earlier in this section, which considered a simplified setting involving only two specific modes (the fundamental and its first harmonic). Recall that by the simple analysis based on the finger tip function $T(2n,n)$, we expected that the interfacial patterns would present inward pointing fingers of the ferrofluid with broad tips or, depending on the magnitude of $T(2n,n)$, we could see a resulting interface with bifurcated fingers. Note that in Fig. 2 the nonlinear terms force the inward fingers to duplicate, favoring the development of twice the number of fingers in comparison to what is expected by the linear approach. Another interesting nonlinear behavior is unveiled when one increases the value of N_B. For larger values of the magnetic field [Figs. 2(d) and 2(f)] we observe a decrease of the "fundamental mode" magnitude, while the "subharmonic" and "first harmonic" modes tend to

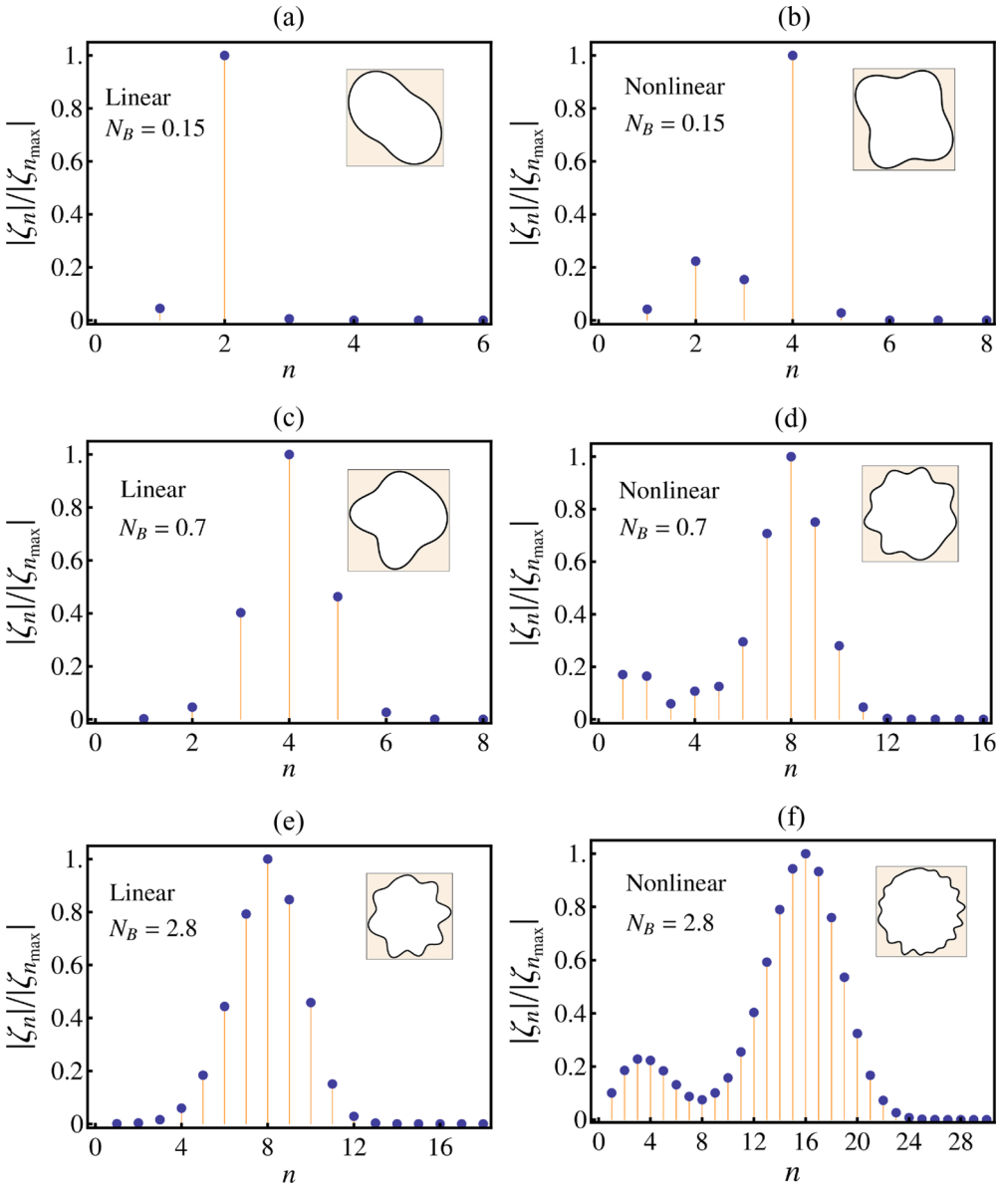

FIG. 2. (Color online) Normalized Fourier amplitudes ($|\zeta_n|/|\zeta_{n_{\max}}|$) as a function of the Fourier modes n, for three values of N_B, and $\chi = 70$. Purely linear (weakly nonlinear) analysis is utilized to plot (a), (c), and (e) [(b), (d), and (f)]. The insets show the corresponding interface shapes at the final time. Notice that linear plots present peaks at $n = n_{\max}$, while weakly nonlinear plots show peaks at $n = 2n_{\max}$.

become the dominant ones in the azimuthal field fingering dynamics. We have verified that the results obtained from Fig. 2 are quite general and can also be obtained for smaller values of χ, as long as the magnetic Bond number has higher magnitude.

III. FULLY NONLINEAR REGIME: STATIONARY PATTERNS

In this section we go beyond the linear and weakly nonlinear stages of the pattern formation process and explore important aspects of the fully nonlinear regime. More specifically, we access the fully nonlinear pattern morphologies through the calculation of the stationary solutions of the ferrohydrodynamic problem. This is done by utilizing the vortex sheet formalism of Hele-Shaw flows [31].

The vortex sheet formulation explores the jump in the tangential component of the fluid velocity as one crosses the interface separating an inner fluid 1 and an outer fluid 2. This approach offers a useful method to probe the fully nonlinear morphology of the arising pattern-forming structures in our azimuthal magnetic field problem. By writing the generalized Darcy's law (2) for both fluids, then by subtracting the resulting expressions, we solve for the vortex sheet strength $\Gamma = (\mathbf{v}_1 - \mathbf{v}_2) \cdot \hat{\mathbf{s}}$ to obtain a dimensionless expression for the vorticity,

$$\Gamma = 2A\mathbf{V} \cdot \hat{\mathbf{s}} + \nabla \left\{ \kappa + \frac{1}{2} \frac{N_B}{r^2} \chi [1 + \chi (\hat{\mathbf{n}} \cdot \hat{\mathbf{e}}_\varphi)^2] \right\} \cdot \hat{\mathbf{s}}, \quad (17)$$

where $\hat{\mathbf{s}}$ is the unit tangent vector along the interface and $\hat{\mathbf{e}}_\varphi$ is the unit vector along the azimuthal direction. In deriving Eq. (17) we have also used the pressure jump (3) described in

Sec. II. In Eq. (17) $A = (\eta_2 - \eta_1)/(\eta_2 + \eta_1)$ is the viscosity contrast, and $\mathbf{V} = (\mathbf{v}_1 + \mathbf{v}_2)/2$ is an average velocity of the interface with $\mathbf{v}_1$ and $\mathbf{v}_2$ being the two limiting values (from both sides of the interface) of the velocity at a given point. Note that the term $(\hat{\mathbf{n}} \cdot \hat{\mathbf{e}}_\varphi)^2$ is reminiscent of the magnetic normal traction contribution in Eq. (3). Equation (17) is made dimensionless by using the same rescaling utilized to nondimensionalize Eqs. (5)–(9).

We are interested in the static solutions of Eq. (17), so $\mathbf{v}_1 = \mathbf{v}_2 = 0$. By taking $\mathbf{V} = 0$ in Eq. (17), and considering the condition of zero vorticity ($\Gamma = 0$), we find that

$$\nabla \left\{ \kappa + \frac{1}{2} \frac{N_B}{r^2} \chi [1 + \chi (\hat{\mathbf{n}} \cdot \hat{\mathbf{e}}_\varphi)^2] \right\} \cdot \hat{\mathbf{s}} = 0. \tag{18}$$

We want to examine the family of planar curves whose curvature satisfies the differential equation (18). These curves are the stationary solutions that balance the competing magnetic and capillary forces at the ferrofluid interface. To find such solutions numerically, we begin by defining the ferrofluid interface as a parameterized curve in terms of polar coordinates r and φ

$$\mathbf{x}(s) = (x(s), y(s)) = r(s)(\cos \varphi(s), \sin \varphi(s)), \tag{19}$$

where the arclength s is taken as the parameter of the curve. From now onward, we will omit the dependence on the parameter s in the equations. In this framing, the interface curvature can be written as [37]

$$\kappa = \left(1 + r_s^2\right)\varphi_s + r(r_s \varphi_{ss} - r_{ss} \varphi_s), \tag{20}$$

where the subscripts indicate derivative with respect to the arclength.

To obtain the stationary shapes, we substitute Eq. (20) into Eq. (18) and solve the resulting expression numerically. However, first we have to write the scalar product $\hat{\mathbf{n}} \cdot \hat{\mathbf{e}}_\varphi$ in Eq. (18) in terms of r and φ. Note that the polar vector $\hat{\mathbf{e}}_\varphi$ is given by

$$\hat{\mathbf{e}}_\varphi = (-\sin \varphi, \cos \varphi), \tag{21}$$

and the normal vector to the interface $\hat{\mathbf{n}}$ can be written as

$$\begin{aligned} \hat{\mathbf{n}} &= (-y_s, x_s) \\ &= -(r_s \sin \varphi + r \varphi_s \cos \varphi, r \varphi_s \sin \varphi - r_s \cos \varphi). \end{aligned} \tag{22}$$

In Eq. (22) we used the expression (19) in polar coordinates. Utilizing (21) and (22) to calculate the scalar product of Eq. (18), we get a very simple relation $\hat{\mathbf{n}} \cdot \hat{\mathbf{e}}_\varphi = r_s$. Therefore, Eq. (18) becomes

$$\kappa_s + \partial_s \left\{ \frac{1}{2} \frac{N_B}{r^2} \chi \left[1 + \chi r_s^2\right] \right\} = 0. \tag{23}$$

For details about the numerical method used to solve equations like Eq. (23), see, for instance, Refs. [38–40].

Figure 3 illustrates a collection of representative stationary solutions for the problem of a fluid bubble surrounded by ferrofluid under the influence of a azimuthal magnetic field. In the top row of Fig. 3 the magnetic susceptibility is $\chi = 5$ and N_B takes increasingly larger values from left to right: $N_B = 3.03 \times 10^{-1}, 4.01 \times 10^{-1}$, and 5.89×10^{-1}. In the middle row $\chi = 10$, and $N_B = 5.985 \times 10^{-2}, 7.731 \times 10^{-2}$, and 9.635×10^{-2}. Finally, in the bottom row $\chi = 70$, and $N_B = 1.053 \times 10^{-3}, 1.287 \times 10^{-3}$, and 1.850×10^{-3}. We emphasize that all patterns illustrated in Fig. 3 are stationary shapes and *not* a time evolving sequence of events.

We advance by discussing the main morphological features of the stationary patterns shown in Fig. 3. First, we observe that all patterns in the first column present inward-pointing fingers with blunt tips. In some cases (second column), these flat tips show an evident tendency to split. These fully nonlinear findings are consistent with the weakly nonlinear prediction made in Sec. II B, where we used the finger tip function approach and prognosticated the tendency toward fingertip broadening and splitting. In addition, we verify that the outward pointing fingers of the nonmagnetic bubble grow as inflated, balloonlike shapes. This occurs because the applied magnetic field decreases with radial distance and, consequently, makes the interface more stable at that points. This behavior leads to a reduction of the curvature of the outward pointing fingers in comparison with the curvature of the inward pointing ones since they are located closer to the current-carrying wire [see Eq. (18)]. Moreover, the magnetic traction term proportional to $(\hat{\mathbf{n}} \cdot \hat{\mathbf{e}}_\varphi)^2$ in Eq. (18) is maximized as $\hat{\mathbf{n}}$ is collinear to $\hat{\mathbf{e}}_\varphi$ so, at the side of the fingers, a larger amount of ferrofluid tend to flow outward to the interface, making the outer fingering structure to become more inflated. Finally, for larger values of χ and N_B, one can see the formation of asymmetric structures, made of two balloons of different sizes and shapes (rightmost pattern in the bottom row). This asymmetry could be attributed to an enhanced nonlinear growth of the mode $n = 1$ [26].

In Fig. 3, one can also notice that the resulting stationary shapes arise as n-fold structures, where for a given χ, the number of fingers decrease for larger values of N_B. This is in opposition to the behavior predicted by the linear stability analysis [see Eq. (10)]. However, this finding is not really surprising: The structures presented in Fig. 3 exhibit strong nonlinear effects that cannot be accessed by a linear approach. One possible explanation for the decrease of the number of fingers for increasingly larger N_B could be given by one of our weakly nonlinear results, where we observed that the increasing of the magnetic Bond number promoted an accentuated growth of the amplitude of the subharmonic Fourier mode [see Figs. 2(d) and 2(f)]. Now, since we are dealing with a fully nonlinear regime, by increasing N_B it is in principle possible to observe a significant growth of lower Fourier modes in comparison to the fastest growing modes predicted by the linear stability analysis. Therefore, these lower modes could eventually dominate the dynamics and dictate the resulting number of fingers in the emerging fully nonlinear patterns.

If the susceptibility takes larger values (second and third rows in Fig. 3) the number of fingers does not change, but their morphology is modified. First, note that by increasing χ the equilibrium outward pointing shapes become even more "swollen." In contrast, the inward pointing fingers grow toward the origin, presenting a flat tip that can bifurcate for higher values of N_B. Finally, when $\chi = 70$ and $N_B = 1.053 \times 10^{-3}$, this behavior induces a topological singularity, implying in interface pinch-off (see the first figure in the bottom row). Similar pinch-off events have been previously detected in the stationary solutions obtained for the rotating Hele-Shaw

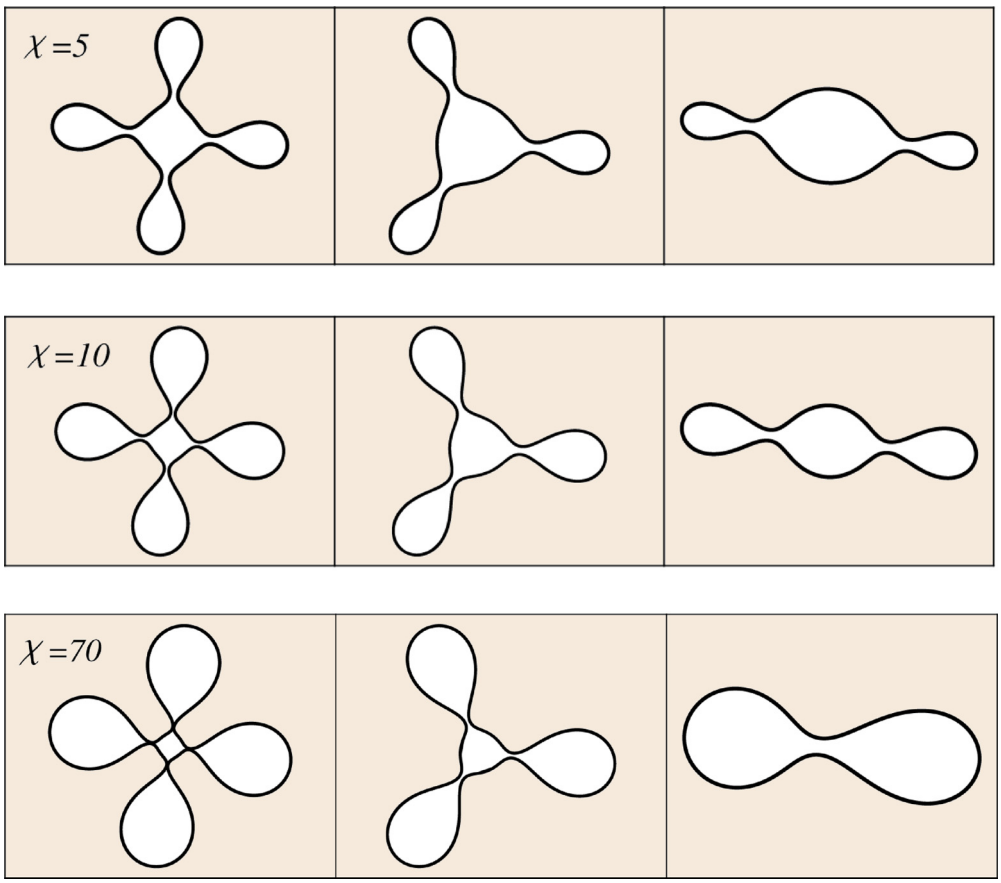

FIG. 3. (Color online) Typical stationary shape solutions for a nonmagnetic fluid bubble surrounded by ferrofluid, considering three increasingly larger values of the magnetic susceptibility χ. The intensity of the magnetic Bond number N_B increases from left to right.

problem with nonmagnetic fluids [38], as well as in the confined radial magnetic field [36] problem with ferrofluids.

IV. CONCLUSIONS

The azimuthal magnetic field configuration originated by a straight current-carrying wire has a long history in the development of interfacial instabilities in ferrofluids. Regarding free surface flows, it is responsible for the well-known conical meniscus instability and more recently has been used to induce the formation of solitons in magnetic fluids. In the context of confined Hele-Shaw flows, the great majority of existing studies focus on the utilization of the azimuthal field as a controlling parameter in order to stabilize ferrofluid interfaces that would otherwise be unstable (i.e., in rotating or lifting Hele-Shaw flows).

In this work, we have explored a different aspect of the azimuthal magnetic field during spatially constrained ferrofluid displacements in Hele-Shaw geometry. Here we concentrated our attention on a situation in which the azimuthal field acts in a destabilizing manner. More specifically, we considered the emergence of ferrohydrodynamic instabilities at an initially circular interface separating a nonmagnetic fluid of negligible viscosity, surrounded by a viscous ferrofluid. In this setting, a current-carrying wire is placed normal to the Hele-Shaw cell plates and passes through the center of the nonmagnetic fluid bubble. It turns out that the azimuthal field presents a natural radial gradient, so a magnetic force pointing radially inward arises, attracting the ferrofluid to the wire. As a result, the two-fluid interface deforms, inducing the formation of interfacial patterns driven by the azimuthal magnetic field.

To investigate the pattern-forming phenomena at early linear stages, as well as at the onset of nonlinear effects, we carried out a mode-coupling analysis of the system. The linear dispersion relation readily reveals that the azimuthal magnetic field is indeed destabilizing, competing with stabilizing surface tension effects. On the other hand, our weakly nonlinear results offer useful analytical insights into the typical interfacial features of the interface up to quadratic nonlinearities. By considering the interplay of a small number of interacting modes (via the finger tip function approach) we have been able to predict that the invading fingers of the ferrofluid tend to be flat and blunt at their tips, admitting the occurrence of finger tip bifurcation. This finger duplication process has been confirmed, even if many participating modes are present. Under such multimode circumstances, we have found that a "first harmonic" mode ($n = 2n_{\max}$) has the largest amplitude and is naturally selected by the weakly nonlinear dynamics. Enhanced growth of a "subharmonic" mode ($n = n_{\max}/2$) has been detected for higher values of the magnetic Bond number.

Finally, a vortex sheet formalism has been employed to address fully nonlinear aspects of the emerging interfacial shapes. In this scenario, we have found stationary solutions

for the interface when magnetic forces are equally balanced by surface tension effects. The resulting typical steady shapes present flat-tip penetrating ferrofluid fingers, separated by balloon-shaped structures of the nonmagnetic fluid. We have also observed that these inflated fingers of the nonmagnetic fluid may pinch off at their basis.

As a natural extension of this work, it would be of interest to study of the development of fully nonlinear, *time-dependent* interfacial fingering structures through intensive conformal mapping, boundary-integral, or phase-field numerical simulations.

ACKNOWLEDGMENTS

We thank CNPq and FACEPE (through PRONEM Project No. APQ-1415-1.05/10) for financial support. E.O.D. acknowledges financial support from FACEPE through PPP Project No. APQ-0800-1.05/14.

[1] R. E. Rosensweig, *Ferrohydrodynamics* (Cambridge University Press, Cambridge, 1985).
[2] E. Blums, A. Cebers, and M. M. Maiorov, *Magnetic Fluids* (de Gruyter, New York, 1997).
[3] See, for instance, D. Andelman and R. E. Rosensweig, J. Phys. Chem. B **113**, 3785 (2009); J.-C. Bacri and F. Elias, in *Morphogenesis—Origins of Patterns and Shapes*, edited by P. Bourgine and A. Lesne (Springer, New York, 2011); I. Torres-Díaz and C. Rinaldi, Soft Matter **10**, 8584 (2014).
[4] M. D. Cowley and R. E. Rosensweig, J. Fluid Mech. **30**, 671 (1967).
[5] R. Friedrichs and A. Engel, Phys. Rev. E **64**, 021406 (2001).
[6] R. Richter and I. V. Barashenkov, Phys. Rev. Lett. **94**, 184503 (2005).
[7] C.-Y. Chen, W.-K. Tsai, and J. A. Miranda, Phys. Rev. E **77**, 056306 (2008).
[8] S. Bohlius, H. Pleiner, and H. R. Brand, Prog. Theor. Phys. **125**, 1 (2011).
[9] J. V. I. Timonen, M. Latikka, L. Leibler, R. H. A. Ras, and O. Ikkala, Science **341**, 253 (2013).
[10] J. L. Neuringer and R. E. Rosensweig, Phys. Fluids **7**, 1927 (1964).
[11] D. A. Krueger and T. B. Jones, Phys. Fluids **17**, 1831 (1974).
[12] J.-C. Bacri, R. Perzynski, D. Salin, and F. Tourinho, Europhys. Lett. **5**, 547 (1988).
[13] T. John, D. Rannaucher, and A. Engel, J. Magn. Magn. Mater. **309**, 31 (2007).
[14] T. John, K. May, and R. Stannarius, Phys. Rev. E **83**, 056308 (2011).
[15] V. G. Bashtovoi and R. A. Foigel, Magnetohydrodynamics (NY) **19**, 160 (1983).
[16] V. G. Bashtovoi, A. Rex, and R. Foigel, J. Magn. Magn. Mater. **39**, 115 (1983).
[17] D. Rannacher and A. Engel, New J. Phys. **8**, 108 (2006).
[18] E. Bourdin, J.-C. Bacri, and E. Falcon, Phys. Rev. Lett. **104**, 094502 (2010).
[19] P. G. Saffman and G. I. Taylor, Proc. R. Soc. Lond. Ser. A **245**, 312 (1958).
[20] For review articles on this topic, see D. Bensimon, L. P. Kadanoff, S. Liang, B. I. Shraiman, and C. Tang, Rev. Mod. Phys. **58**, 977 (1986); G. M. Homsy, Annu. Rev. Fluid Mech. **19**, 271 (1987); K. V. McCloud and J. V. Maher, Phys. Rep. **260**, 139 (1995); J. Casademunt, Chaos **14**, 809 (2004).
[21] A. O. Tsebers and M. M. Maiorov, Magnetohydrodynamics (NY) **16**, 21 (1980).
[22] A. O. Cebers, Magnetohydrodynamics (NY) **17**, 113 (1981).
[23] S. A. Langer, R. E. Goldstein, and D. P. Jackson, Phys. Rev. A **46**, 4894 (1992).
[24] D. P. Jackson, R. E. Goldstein, and A. O. Cebers, Phys. Rev. E **50**, 298 (1994).
[25] J. A. Miranda, Phys. Rev. E **62**, 2985 (2000).
[26] D. P. Jackson and J. A. Miranda, Phys. Rev. E **67**, 017301 (2003).
[27] S. A. Lira, J. A. Miranda, and R. M. Oliveira, Phys. Rev. E **82**, 036318 (2010).
[28] J. A. Miranda and R. M. Oliveira, Phys. Rev. E **69**, 066312 (2004).
[29] C.-Y. Chen, S.-Y. Wu, and J. A. Miranda, Phys. Rev. E **75**, 036310 (2007).
[30] J. A. Miranda and M. Widom, Physica D **120**, 315 (1998).
[31] G. Tryggvason and H. Aref, J. Fluid Mech. **136**, 1 (1983).
[32] L. Paterson, J. Fluid Mech. **113**, 513 (1981).
[33] J.-D. Chen, J. Fluid Mech. **201**, 223 (1989); Exp. Fluids **5**, 363 (1987).
[34] O. Praud and H. L. Swinney, Phys. Rev. E **72**, 011406 (2005).
[35] S. W. Li, J. S. Lowengrub, J. Fontana, and P. Palffy-Muhoray, Phys. Rev. Lett. **102**, 174501 (2009).
[36] R. M. Oliveira, J. A. Miranda, and E. S. G. Leandro, Phys. Rev. E **77**, 016304 (2008).
[37] H. W. Guggenheimer, *Differential Geometry* (Dover, New York, 1977).
[38] E. S. G. Leandro, R. M. Oliveira, and J. A. Miranda, Physica D **237**, 652 (2008).
[39] G. Arreaga, R. Capovilla, C. Chryssomalakos, and J. Guven, Phys. Rev. E **65**, 031801 (2002).
[40] P. A. Djondjorov, V. M. Vassilev, and I. M. Mladenov, Int. J. Mech. Sci. **53**, 355 (2011).